Reac Kinet Mech Cat (2015) 114:433–449
DOI 10.1007/s11144-014-0821-0

Effects of pretreatment on iron-based catalysts for forming light olefins via Fischer–Tropsch synthesis

Yi Liu · Jian-Feng Chen · Yi Zhang

Received: 30 September 2014 / Accepted: 16 December 2014 / Published online: 27 December 2014

Abstract The effects of ethylene glycol modified co-precipitation were applied to develop a catalyst with higher activity and selectivity of light olefins in the Fischer–Tropsch synthesis. The catalysts prepared by an ethylene glycol (EG) modified co-precipitation realized smaller and homogeneously distributed catalyst particles as 15–25 nm, which was two times smaller than that of the catalyst prepared from conventional co-precipitation. The Fe/Mn-EG catalyst has higher activity and enhanced selectivity to light olefins, as well as the doubled olefin to paraffin ratio ($C_2^=$–$C_4^=$/C_2^0–C_4^0), comparing to un-pretreated catalyst. Furthermore, the addition of magnesium promoter to the Fe/Mn-EG catalyst inhibits the chain growth ability, and enhances the formation of light olefins ($C_2^=$–$C_4^=$), realizing the high selectivity of light olefins as 50.1 %. The properties of catalyst structure, active phase, reduction and carburization of obtained catalysts were characterized by N_2 physisorption, XRD, SEM, XPS, TPR and DRIFTS measurements.

Keywords Fischer–Tropsch synthesis · Iron-based catalysts · Ethylene glycol · Magnesium · Syngas

Electronic supplementary material The online version of this article (doi:10.1007/s11144-014-0821-0) contains supplementary material, which is available to authorized users.

Y. Liu · Y. Zhang
State Key Laboratory of Organic–Inorganic Composites, Department of Chemical Engineering, Beijing University of Chemical Technology, Beijing 100029, China

J.-F. Chen · Y. Zhang (✉)
Research Centre of the Ministry of Education for High Gravity Engineering and Technology, Beijing University of Chemical Technology, Beijing 100029, China
e-mail: yizhang@mail.buct.edu.cn

Introduction

The Fischer–Tropsch synthesis (FTS) converts syngas derived from natural gas, coal and biomass into a large variety of products such as paraffins, olefins, alcohols via catalytic surface polymerization. In recent years, due to the shortage of crude oil reserves and environmental constraints, there has been increasing global concern over the FTS in both academia and industry [1, 2]. Relative to other FTS catalysts, iron-based catalysts are well known for their high selectivity of light olefins and low costs. In addition, iron-based catalysts might be the best candidates for converting syngas to clean liquid fuels and olefins, because of their higher activity of water gas shift (WGS) reaction enabling the use of a CO-rich syngas feed derived from coal [3], lower methane selectivity and a flexible option as a working catalyst [4, 5].

Generally, the most common method for the synthesis of iron-based FTS catalysts is co-precipitation from iron salt solutions. Many iron oxide precursors, for example, are synthesized by adding an iron nitrate solution to a sodium carbonate solution [6]. However, the average crystallite size of the hematite phase in precipitated iron-based FTS catalysts is typically large. It is well known that nano-materials may offer different morphology and enhanced surface area that, in theory, should yield better reaction rates due to an increase in available active sites. Recent studies with nano-sized metals under typical FTS conditions have shown that those nano-sized iron particles were essential to achieve high FTS activity and good stability [3, 7, 8]. Iglesia et al. [9] reported that incorporating Zn into iron-based catalysts resulting in forming $ZnFe_2O_4$ species, increases the surface area of precipitated oxide precursors by inhibiting sintering during thermal treatment and activation in H_2/CO reactant mixtures, leading to higher FTS rates than on ZnO-free precursors. However, this effect cannot extend to different catalyst systems which incorporate with other promoters. Ding et al. [7] investigated the preparation of Fe_2O_3–Al_2O_3 nano-catalysts, in which the iron oxide nano-particles have a very narrow size distribution, are surrounded by the Al_2O_3 matrix resulting in stable nanostructures, contributing to high catalytic activity, higher olefin selectivity and lower CO_2 selectivity.

Meanwhile, iron-based catalysts often contain small amounts of potassium and other metals such as manganese, copper and magnesium as promoters to improve their activity and selectivity [10, 11]. It is clearly reported that potassium can facilitate the WGS reaction and the presence of Cu in Fe-based catalyst can facilitate the reduction of Fe, resulting in high activity of catalysts [9, 10]. Recently, Luo et al. [12] compared group II alkali-earth metal-promoted iron-based catalysts with potassium-promoted and un-promoted catalysts under medium pressure conditions, which are suitable for slurry phase reactor operations. They showed that the promoted catalysts with magnesium exhibit lower FTS activity and chain growth factor compared to potassium-promoted iron catalyst. In addition, it was found that the magnesium promoter has a negative effect on WGS activity. Gallegos et al. [13] studied the Fe/SiO_2–MgO catalysts for FTS reaction. They showed that the rate of hydrocarbon formation increases with increasing MgO content. Yang et al. [10] reported that MgO is an effective promoter in shifting FTS selectivity to lighter molecular weight hydrocarbons. However, Pour et al. [14] found that Mg

promoter can improve the CO conversion and WGS reaction, suppress the formation of methane.

In this study, the preparation of nano-sized iron-based catalysts, using modified co-precipitation process by ethylene glycol, is proposed here. The effects of ethylene glycol pretreatment and addition of magnesium to EG promoted catalysts on activity and light olefin selectivity were investigated using N_2 physisorption, XRD, SEM, TEM, XPS, TPR and DRIFTS measurements.

Experimental

Catalyst preparation

The catalyst precursors used in the present work were prepared by co-precipitation method. A mixture containing $Fe(NO_3)_3{\cdot}9H_2O$ (99.9 %, Tianjing Chemical Co., P.R. China), KNO_3 (99.9 %, Beijing Chemical Co., P.R. China), $Cu(NO_3)_2{\cdot}3H_2O$ (99.9 %, Beijing Chemical Co., P.R. China) and $Mn(NO_3)_2{\cdot}4H_2O$ (Aldrich 99.99 %) with an Fe/Cu/Mn/K molar ratio of 200/30/100/5 was premixed and pretreated using ethylene glycol for 1 h at 333 K in a round bottomed flask. Aqueous Na_2CO_3 (99.9 %, Beijing Chemical Co., P.R. China) was used as a precipitating agent. Both solutions were simultaneously added to a precipitating batch containing 300 ml of distilled water at the start, and its rate was controlled in order to keep the pH of the slurry at 8.0 ± 0.2 during precipitation. The resulting precipitate was first filtered and then washed with warm distilled water. The precursor was then dried in air at 393 K for 12 h, and then calcined in air from room temperature to 673 K in 3 h and maintained at 673 K for 2 h. The obtained catalyst was denoted as Fe/Mn-EG. For comparison, a catalyst precursor with the same composition but pretreated using distilled water was prepared by the same method. The sample was denoted as Fe/Mn-H_2O, which is used as a reference.

In addition, Mg-promoted catalyst with a composition of 200 Fe/30 Cu/100 Mn/100 Mg/5 K was prepared by the same method as Fe/Mn-EG catalyst, the sample was denoted as Fe/Mn/Mg-EG.

The composition of all obtained catalysts was determined by ICP, and it is almost 98 % of stoichiometric value for each element.

Catalyst characterization

The BET surface area, pore volume, and average pore diameter of the fresh catalysts were obtained via nitrogen physisorption at 77 K using Micrometrics ASAP 2010 equipment. Each sample was degassed at 573 K for 6 h prior to the measurement.

An X-ray diffractometer (XRD, SHIMADZU XRD-6000) was used to detect crystalline size of the fresh catalysts. The crystalline average size was calculated by $L = K\lambda/\Delta(2\theta)\cos\theta_0$,where L is the crystalline size, K is a constant ($K = 0.9$), λ is the wavelength of X-ray ($CuK_\alpha = 0.154$ nm), and $\Delta(2\theta)$ is the width of the peak at half height.

SEM images of the fresh catalysts were determined by a Hitachi S-4700 microscope. The specimen was prepared by ultrasonically suspending the catalyst powder in ethanol. A drop of the suspension was deposited on a cover slip and dried in air. For TEM measurement using Hitachi H-800 microscope, the specimen was prepared by ultrasonically suspending the catalyst powder in ethanol. Then a drop of the suspension was brought onto a holey carbon film on a copper grid and dried in air.

H_2-Temperature programmed reduction (H_2-TPR) experiments were carried out in a quartz tube reactor using 0.05 g calcined catalysts. The reducing gas, a mixture of 10 % H_2 diluted by Ar, was fed via a mass flow controller at 30 ml/min and the temperature was increased from 303 K until 1,073 K at a rate of 8 K/min. The effluent of reactor passed through a 5 Å molecular sieve trap to remove produced water, before reaching TCD. The conditions of CO-TPR experiment are similar to those for H_2-TPR, and the only difference is that a liquefied nitrogen bath was used to remove CO_2 formed during the carbon monoxide reduction.

In situ diffuse reflectance infrared Fourier transform (DRIFT) spectra were collected on a BRUKERVERTEX 70V FT-IR spectrometer equipped with a diffuse reflectance attachment and an MCT detector. The catalyst powder of 18 mg was contained in a diffuse reflectance infrared cell with a KBr window. In situ absorbance spectra were collected using 32 scans at 2 cm^{-1} resolution. The effluent of feed gas (95 % CO/5 % Ar) passed through an active carbon trap to remove iron carbonyl before reaching the in situ reaction system. Before the adsorption of CO, the passivated catalyst sample was treated in situ in a N_2 stream flowing at 30 ml/min at 298 K for 30 min, 573 K for 30 min, and then was reduced in a CO stream flowing at 30 ml/min at 573 K and atmospheric pressure for 30 min. The catalyst sample was swept by N_2 at 573 K for 30 min; then the catalyst sample was cooled down in N_2 to 298 K for 1 h. The spectra were obtained at room temperature after the exposure of catalyst to CO/Ar at a ratio of 95/5 flowing at a total rate of 30 ml/min for 10 min, followed by sweeping in N_2 for 30 min.

The XPS analysis of the fresh catalysts was performed on a Thermo Fisher Scientific ESCALAB 250 spectrometer. The spectra were excited by themonochromatized Al K_α source (1,486.6 eV). The analyzer operated in the constant analyzer energy (CAE) mode. Survey spectra were measured at 30 eV pass energy. The peak positions were corrected for sample charging by setting the C 1 s binding energy at 284.8 eV.

Catalyst testing

The FTS reaction was carried out in a continuous-flow type fixed-bed reactor (SUS 316 L, 8 mm i.d.). The reaction conditions were P (total) = 1.0 MPa, $CO/H_2 = 1$, $W_{cat.}/F_{(CO+H2+Ar)} = 5$ g-cat h mol^{-1}, T = 553 K. The reactor temperature was measured with a K-type thermocouple buried in the catalytic bed. Flow rates were controlled using a Brooks 5850 TR Series mass flow controller. The feed gas consisted of Ar (4.99 %), CO (47.5 %) and H_2 (47.6 %). 0.5 g catalyst mixed with 1.0 g quartz sand was placed in the reactor tube and reduced in situ at 573 K for 10 h in the flow of feed gas at 0.1 MPa, followed by cooling down to 353 K in N_2.

When the reaction temperature was reached, pressurized syngas was introduced and the reaction was carried on continuously for more than 20 h.

The effluent gas from the reactor was analyzed by on-line gas chromatography (GC). A thermal conductivity detector (TCD) was used to analyze gaseous products (CO, CO_2 and CH_4). Light hydrocarbons (C_1–C_5) were analyzed on-line by another GC with flame ionization detector (FID) using a Porapak-Q column. The analyses of hydrocarbons dissolved in the solvent and cooled in the trap were carried out with GC-FID using silicone SE-30 column. The mass balance of various reactions were calculated, which were almost 95 % based on carbon mole for all reactions. The selectivity to oxygenates was below 1 % C and has been excluded from the reported product selectivities.

Results and discussion

Structural properties of the catalysts

The textural properties, pore size distributions and elemental compositions for stoichiometric and surface of the iron-based catalysts are shown in Table 1 and Fig. S1. It is apparent that the precursors pretreated by ethylene glycol remarkably

Table 1 Textural properties of the fresh catalysts

Catalysts	Fe/Mn-H_2O	Fe/Mn-EG	Fe/Mn/Mg-EG
BET surface area (m^2/g)[a]	129	178	154
BET surface area (m^2/g)[b]	98	160	129
Pore volume (cm^3/g)	0.21	0.38	0.23
Averagepore diameter (nm)	4.89	7.83	4.55
Particle size (SEM, nm)	44.9	23.0	21.3
Iron oxide size (TEM, nm)[c]	2.51	1.35	1.18
Mn/Fe atomic ratio			
Stoichiometric	0.5	0.5	0.5
Surface[d]	0.82	0.92	0.69
Mg/Fe atomic ratio			
Stoichiometric	–	–	0.5
Surface[d]	–	–	1.02
$A(Fe^{3+} + Fe^{2+})/A^{e}_{total}$	0.68	0.59	0.61

[a] Measured from the fresh catalysts

[b] Measured from the reduced catalysts

[c] Measured from the calcined catalysts

[d] Determined by XPS

[e] Surface iron composition for various catalysts determined by in situ DRIFT; Calculated by CO adsorption peak area; A_{total}: $A(Fe^{3+} + Fe^{2+}) + A(Fe^{0})$

influence the BET surface area, pore volume and pore size distribution. It can be seen that the BET surface area of the fresh Fe/Mn-H_2O catalyst is about 129 m^2/g, while for the fresh Fe/Mn-EG catalyst, the surface area increases from 129 to 178 m^2/g. Meanwhile, the average pore size and pore volume also increase significantly. However, by addition of magnesium promoter, the BET surface area, pore volume and average pore size of the catalysts decrease. After the activation, the BET surface areas of the reduced catalysts slightly decreased, but it exhibited a same trend comparing to the results of fresh catalysts. Based on the above findings, it can be concluded that the pretreatment by ethylene glycol changes the structure of the catalyst too much, and addition of Mg adjusts pretreatment effects on the catalyst structure, resulting in relatively high specific surface area and smaller pore size those are advantageous to forming light hydrocarbon in FTS. The N_2 adsorption–desorption isotherms of the fresh iron-based catalysts are displayed in Fig. S2. The isotherm exhibit a hysteresis loop typical for capillary condensation in the mesoporous materials.

The powder X-ray diffraction patterns for the fresh catalysts are shown in Fig. 1. The pattern of all the catalysts did not have characteristic peaks of Fe_2O_3 or MnO_x, indicating that both MnO_x and Fe_2O_3 phases had incorporated Fe^{3+} and Mn^{x+} ions, respectively, in their lattice and formed mixed lattices [2, 15, 16]. Due to the complicated components of the catalysts in the present work, it is difficult to distinguish the diffraction peaks of the mixed oxide. However, it is found that the peak intensity of pretreated catalyst is weaker than that of the un-pretreated catalyst, suggesting that the crystallite size of Fe/Mn-EG catalyst is smaller than Fe/Mn-H_2O catalyst, as shown in Fig. 1. Hence, it can be concluded that pretreatment by

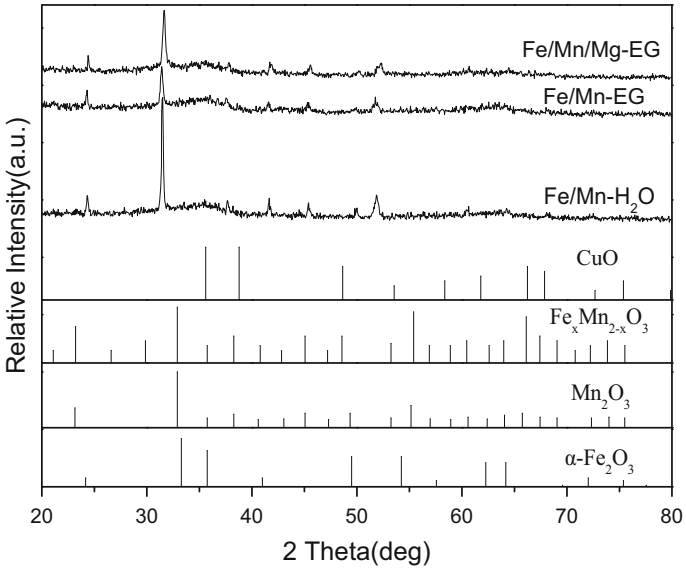

Fig. 1 The XRD patterns of the fresh catalysts

ethylene glycol inhibits the aggregation of the iron-based catalyst during co-precipitation, and leads to the formation of the relatively smaller catalyst particles. For the catalyst with magnesium promoter, the crystallite size of metal was further decreased. According to the literature [10, 13], the addition of a certain level of magnesium promoter into the catalysts can enhance the dispersion of Fe_2O_3 phase and modify the metallic crystal size, which is well agree with our results.

The XRD patterns of the activated catalysts by syngas are presented in Fig. S3. It can be found that iron carbide phases are formed for all reduced catalysts. According to the JCPDS card, the most intense peak of iron carbide species is about 42.7° [17]. Peak assignment was based on the characteristic Bragg angles of θ-Fe_3C (JCPDS 76-1877) at 78.0° and 70.1°, which are not present in the diffractogram of the sample χ-$Fe_{2.5}C$ (JCPDS 36-1248) [18]. As shown in Fig. S3, for Fe/Mn-EG catalyst, the peak intensity of iron carbide was similar to that of Fe/Mn-H_2O catalyst. However, the iron carbide species of Fe/Mn/Mg-EG catalyst shows very weak intensity and broad peak. Because the peak intensity of XRD patterns is always influenced by the particle size and content of sample, it is difficult to identify the particle size of iron carbide, due to complex formation and composition of formed iron carbide.

The XRD patterns of the catalysts after the FTS reaction with syngas are presented in Fig. S4. For all the samples, the main peaks can be assigned to the presence of iron carbides [17, 18], indicating that Fe_2O_3 is almost completely converted into the Fe carbides during the FTS reaction. Due to the poor crystallographic form of iron carbides, it is impossible to specify which carbide is obtained under these conditions from the XRD patterns. However, the peak intensity among the samples exhibited a same trend comparing to the results of fresh and activated catalysts.

Fig. 2 shows the SEM images of the fresh catalysts. Significant differences in particle size have been observed among the calcined samples. The Fe/Mn-EG catalyst exhibited remarkable smaller particle size and distributed homogeneously (Fig. 2b); the particle size distribution indicates the average size of catalyst particle was ~23.0 nm, calculated from the statistical SEM data over 100 particles. While in the case of Fe/Mn-H_2O, larger catalyst particle aggregated into even larger clusters (Fig. 2a), the average size was ~44.9 nm, as tabulated in Table 1. Therefore, it is proved that the pretreatment of precursors by ethylene glycol extremely restrained the aggregation of catalyst particles, resulting in decreased particle size and homogeneous particle distribution. On the other hand, it is considered that during the calcination step, the heat uniformly released from thermal decomposing of oxyl group derived from ethylene glycol was quickly absorbed by the precursor of catalyst to supply energy for decomposition of nitrates, which efficiently restrained the aggregation of the complex iron manganese oxides, resulting in smaller particle size [19, 20]. For the Fe/Mn/Mg-EG catalyst, it is found that the addition of magnesium promotes the dispersion of particles, the average size decreased from ~23.0 to ~21.3 nm (Fig. 2c).

The TEM micrographs of the calcined catalysts are shown in Fig. 2d–f. The average size of iron oxide particle was 1.35 nm in the Fe/Mn-EG catalyst when it was pretreated by ethylene glycol, which increased to 2.51 nm for Fe/Mn-H_2O catalyst. Furthermore, the average size of iron crystallites of the Fe/Mn/Mg-EG

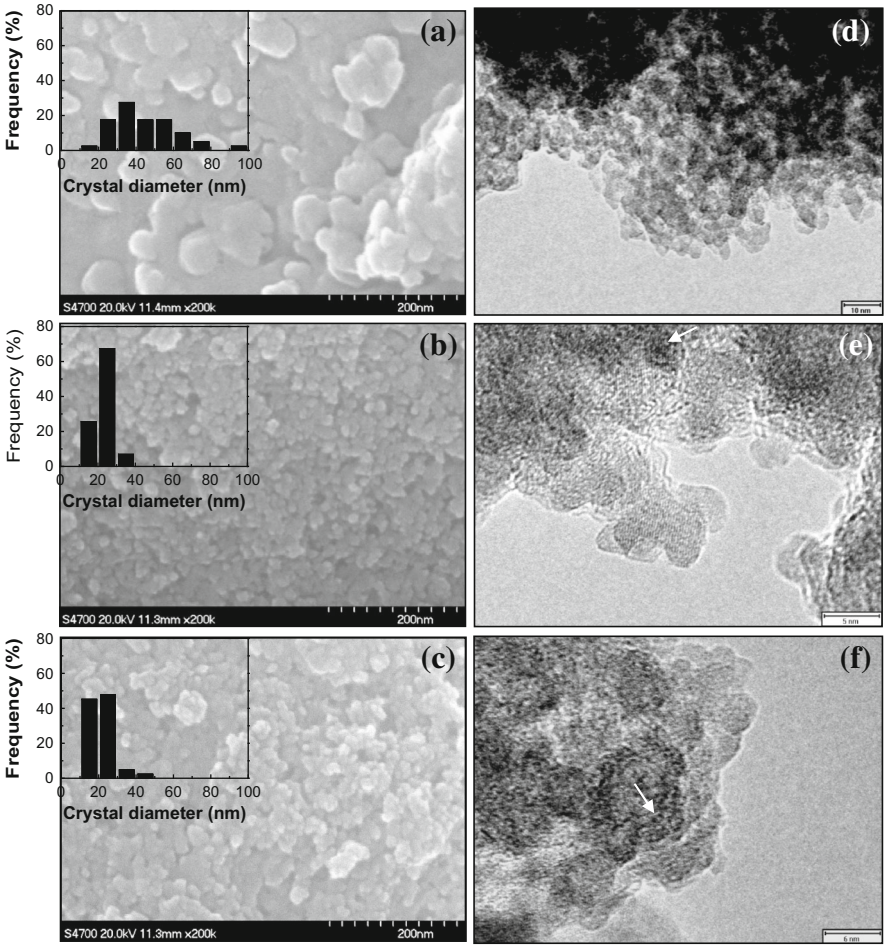

Fig. 2 SEM images of various fresh catalysts, and the size distribution of nanoparticles was shown in the left inset: **a** Fe/Mn-H_2O catalyst; **b** Fe/Mn-EG catalyst; **c** Fe/Mn/Mg-EG catalyst; The TEM images of various calcined catalysts: **d** Fe/Mn-H_2O catalyst; **e** Fe/Mn-EG catalyst, **f** Fe/Mn/Mg-EG catalyst

catalyst was 1.18 nm, much smaller than those of Fe/Mn-EG catalyst (Table 1). These results strongly suggest that the ethylene glycol pretreated catalyst facilitated the dispersion of active crystallites, and the addition of Mg further enhance this effect.

Chemical composition and electronic properties

The XPS study was carried out to determine the chemical composition and valence state of the elements on the surface of the obtained catalysts. The spectra recorded are shown in Fig. 3. Fe2p XPS spectra indicate that Fe species are characteristic of trivalence in Fe_2O_3 [21]. It is also found that the Mn/Fe and Mg/Fe atomic ratio on

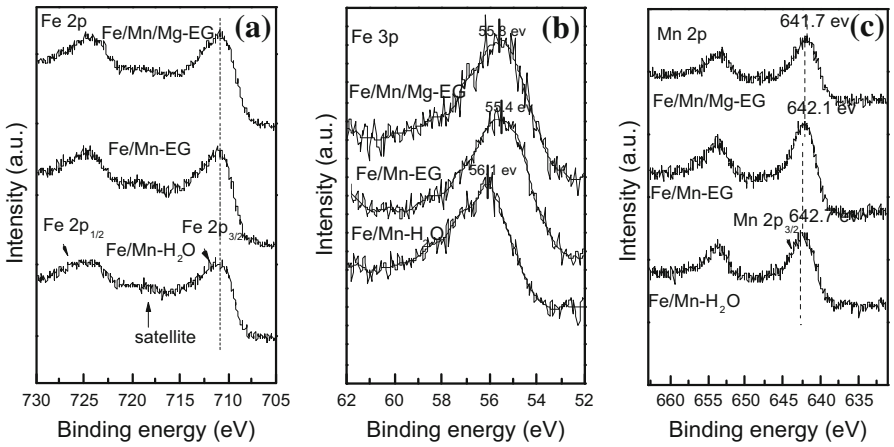

Fig. 3 **a** Fe2p, **b** Fe3p, and **c** Mn2p XPS spectra of various fresh catalysts

the catalysts surface is much larger than the stoichiometric ratio for all the catalysts, which indicates that the promoters are enriched on the catalyst surface after the catalyst being calcined. Furthermore, it was observed that the pretreatment of precursors by ethylene glycol remarkably increase the Mn/Fe atomic ratio on the catalyst surface, increase from 0.82 of Fe/Mn-H_2O to 0.92 of Fe/Mn-EG. However, the addition of magnesium promoter significantly decrease the Mn/Fe atomic ratio on the catalyst surface, as compared in Table 1, indicating that added Mg effectively restructures the surface chemical composition and adjusts the interaction between iron and promoters. On the other hand, the peak intensity of Fe/Mn-EG and Fe/Mn/Mg-EG catalyst is stronger than that of Fe/Mn-H_2O catalyst due to more iron surface atom on the catalysts, indicating that the dispersion of iron is better for EG pretreated catalyst.

XPS was also used to probe the metal electronic structures in all catalysts. As shown in Fig. 3a, there is no obvious difference in chemical shift in the Fe2p region. It is well known that electrons in the outer Fe3p core level are more sensitive to the variation of electronic structures [22]. Thus, the Fe3p XPS spectra were used to further probe the changes in electronic structure of Fe species in catalysts. The XPS spectra of Fe3p and Mn2p are shown in Fig. 3b and c.

From Fig. 3b, it can be seen that the binding energies (BEs) of the Fe3p shift to lower values for the Fe/Mn-EG catalyst compared with that for Fe/Mn-H_2O catalyst. At the same time, Mn2p BEs (Fig. 3c) shift to lower values, suggesting that the electron transfer between Fe and Mn atoms was disturbed. The chemical shifts reflect changes in the electron density around the atom of corresponding elements in the samples [23]. It is considered that the electron density of the surface iron atom is higher due to the weakened Fe-support interaction, which would adjust the transfer of electron between iron and support.

However, the addition of the magnesium promoter slightly increased the BEs of the Fe3p, which is still lower than that of Fe/Mn-H_2O catalyst. It is considered that

for Fe/Mn/Mg-EG catalyst, the intensity of Fe–Mn interaction would be adjusted due to the newly formed Fe–Mg interaction, which slightly increases the interaction between iron and support, resulting in increased binding energy of iron surface atom in Fig. 3b.

Temperature programmed reduction

The promotional effect of pretreatment and magnesium on the reduction behavior of the iron-based catalysts was measured by H_2-TPR and CO-TPR. The H_2-TPR profiles of the catalysts are presented in Fig. S5. It is clearly shown that the reduction process of all catalysts occurs in two main stages. The first stage at low temperature (200–400 °C) is attributed to the transformations of $CuO \rightarrow Cu$, $MnO_x \rightarrow MnO$ and $Fe_2O_3 \rightarrow Fe_3O_4$, whereas the second stage at higher temperature (above 500 °C) correspond to the transformation of $Fe_3O_4 \rightarrow Fe$ [10, 11, 24]. It is also found that, for the Fe/Mn-H_2O catalyst, the first stage can be further separated into three reduction peaks, which appeared at 230, 243 and 276 °C. However, in the cases of Fe/Mn-EG catalyst, these reduction peaks overlap into a single peak (ca. 259 °C), and the required temperatures are also apparently decreased. This suggests that the first reduction step is too fast to be separately recorded, indicating that the pretreatment by ethylene glycol enhances the reduction of metal oxide. Furthermore, the peak at the second stage in the TPR of Fe/Mn-EG catalyst also shifts to lower temperature, suggesting that the iron oxide on Fe/Mn-EG catalyst is more easily reduced to Fe at high temperature than that on Fe/Mn-H_2O catalyst.

The possible reason for this phenomenon is complex and diverse. On the one hand, as confirmed by XPS, the Fe–Mn interaction can be effectively weakened by ethylene glycol. Many studies [11, 25] have reported that the strong Fe–Mn interaction suppressed the reduction of α-Fe_2O_3 to Fe_3O_4, stabilized the FeO phase. It agrees well with our results. On the other hand, as displayed in the above BET, XRD, SEM and TEM results, the presence of ethylene glycol restricts the aggregation of crystallites, resulting greater surface area, smaller catalyst particles, and a larger percentage of surface atoms than of bulk iron oxides. Obviously, surface atoms have a higher probability of contact with H_2 during the reduction, and highly dispersed iron oxide nano-particles have been shown to be more easily reduced than bulk iron oxide [22, 26]. Therefore, it can be proposed that the reduction of iron oxides is promoted by the pretreatment of ethylene glycol.

For the catalyst with magnesium promoter, namely Fe/Mn/Mg-EG, the first reduction region shifted to higher temperature. Yang et al. [10] studied the effect of Mg promoter on precipitated Fe/Cu/K/SiO_2 catalysts for FTS, and found that a small amount of magnesium promoter can promote the dispersion of Cu promoter, which improve the reduction of the catalyst, and the excessive magnesium promoter may weaken the interaction between Cu and Fe oxide, resulting in a restraint of the catalyst reduction. In the present work, it is considered that magnesium promoter may weaken the interaction between Cu and Fe oxide, resulting in forming Fe–Mg and Mn–Mg interaction as illustrated in XPS results, leading to a higher reduction temperature of first reduction peak, which mainly contains the reduction of Cu and

Mn oxide. However, the second reduction peak of Fe/Mn/Mg-EG catalyst still located at relatively lower temperature than that of Fe/Mn-H_2O catalyst. It is considered that the weakened interaction of iron and support as founded by XPS contributes to the slightly lower reduction temperature of iron oxide. Therefore, it is proved that the pretreatment by EG significantly influence the properties of obtained catalysts, and addition of Mg effectively adjusts the promotional effects of pretreatment. It is believed that keeping the reducibility of iron and suppressing the reduction of Cu would significantly influence the hydrogenation reaction performance during FTS, especially the hydrogenation of formed olefins.

The CO-TPR profiles of the catalysts are shown in Fig. 4. All the profiles show three peaks. The catalyst is generally reduced and carburized via two main stages under CO atmosphere. The first stage at the temperature of 150–280 °C presents the reduction of hematite (Fe_2O_3) to magnetite (Fe_3O_4), and the follow stage at the temperature of 300–450 °C presents the reduction of magnetite (Fe_3O_4) to iron carbides (Fe_xC) [11, 24], and a shoulder peak appears above 450 °C, which can be ascribed to the deposition of amorphous carbon derived from the Boudouard reaction of CO ($2CO \rightarrow C + CO_2$) [4]. It should be noted that, for Fe/Mn-EG catalyst, both of the two peaks significantly shift to lower temperature, indicating that the pretreatment of ethylene glycol facilitates the reduction and carburization of the catalyst in CO due to the weakened interaction of iron and supports; this is consistent with the results of H_2-TPR.

For Mg promoted catalyst, the first and second reduction peak shifts to high temperature due to adjusted interaction of different elements as mentioned in H_2-TPR. However, the main reduction peak, located from 300 to 450 °C, becomes broader, indicating the reduction of various iron species and forming different iron carbides. In general, the reduction behavior reflects the activation capability of

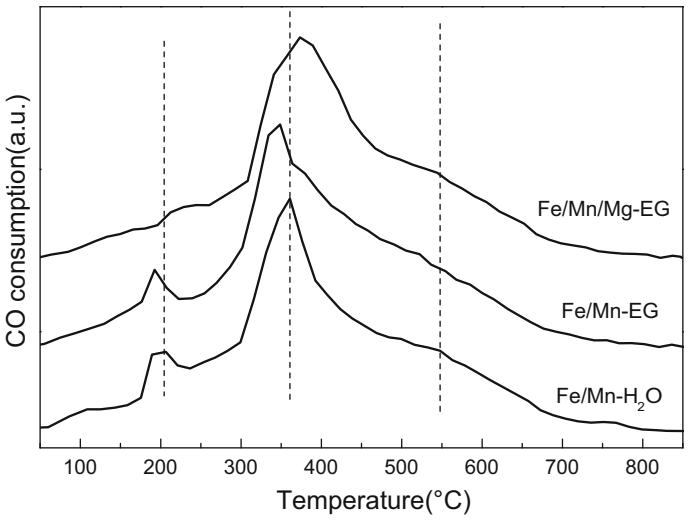

Fig. 4 CO-TPR profiles of various catalysts

catalysts [27]. Hence, the effects of the pretreatment and magnesium promoter on the reduction would directly influence the FTS activity and selectivity.

In situ DRIFT spectra of the catalyst

In situ DRIFT spectra of the adsorbed CO on the reduced catalysts are compared in Fig. S6. In previous reports, a few studies have dealt with infrared spectroscopic investigation of surface species on iron-based catalysts; the assignment of CO adsorption on iron carbides has also been reported little. Different authors studying the adsorption of CO on reduced iron particles (supported or not) ascribe IR bands in the range 2,040–1,980 cm^{-1} to linear CO species adsorbed on Fe^0 sites [28–30]. In this study, iron carbide adsorbed CO species manifested itself by a band at 2,002, 2,006 and 2,021 cm^{-1} for Fe/Mn-H_2O, Fe/Mn-EG and Fe/Mn/Mg-EG catalysts, respectively. In general, the blue shift of this band indicated that the C–O band became strong if the CO adsorbed onto small iron. The band of CO adsorbed on Fe metal in linear mode shifted from 2,002 cm^{-1} for Fe/Mn-H_2O catalyst to 2,006 cm^{-1} for ethylene glycol modified catalyst here, as the iron particle size of ethylene glycol modified catalyst was smaller than that of Fe/Mn-H_2O catalyst, according to the data from SEM and TEM in Table 1, indicating that the addition of ethylene glycol promoted the dispersion of iron. On the other hand, the stronger peaks of linear adsorbed CO, as illustrated in Fig. S6, revealed that CO adsorbed on the EG-modified iron-based catalyst was more active than that on Fe/Mn-H_2O catalyst. Compared to Fe/Mn-EG catalyst, the peak assigned to the linear adsorption of CO on the Fe/Mn/Mg-EG catalyst shifted towards blue side. As was already demonstrated in the previous results, the particle size of the magnesium promoted catalyst was smaller than Fe/Mn-EG catalyst, as shown in Table 1, which would favor the blue shift of the linear adsorption of CO on iron. The results obtained from the DRIFTS spectra agree well with those of XRD, SEM, TEM and TPR.

The bands at 1,915, 1,872 cm^{-1} and 1,941, 1,894 cm^{-1} for Fe/Mn-H_2O and Fe/Mn-EG catalysts, respectively, are attributed to the bridge-type CO adsorbed on Fe^0 sites [31–35]. No bridged adsorption of CO on Fe^0 sites was observed on Fe/Mn/Mg-EG catalyst. The bridge-type adsorbed CO can be easily dissociated to carbon and oxygen, contributing to the FTS activity [36]. For the Fe/Mn-EG catalyst, the peak of the bridged adsorbed CO was much stronger than that on Fe/Mn-H_2O catalyst, indicating that more active bridged adsorbed CO, were formed on the modified catalysts, which were easily dissociated to carbon and oxygen, contributing to the higher reaction rate of FTS. It was considered that the pretreatment by ethylene glycol on iron-based catalyst might form more active interface, stabilizing more bridge-type adsorbed CO which was responsible to some extent for the improvement in FTS activity.

Furthermore, two peaks were obtained at the range of 2,250–2,050 cm^{-1} for all catalysts, which was attributed to the linearly adsorbed CO on Fe (3+) and Fe (2+) species [34]. Jiang et al. [37] reported that some Fe (2+) and Fe (3+) species still exist after the iron sample is reduced in high-pressure H_2 or syngas of 1.2 MPa at 300 °C. To estimate the reduction degree of the catalysts, the ratio of $(Fe^{3+} + Fe^{2+})/(Fe^{3+} + Fe^{2+} + Fe^{0+})$ species was calculated from the peak area of

adsorbed CO, as shown in Table 1. Consequently, the higher ratio of (Fe^{3+} + -Fe^{2+})/(Fe^{3+} + Fe^{2+} + Fe^{0+}) species means to the lower reduction degree. It can be found that the amount of higher valence state iron ion is highest for Fe/Mn-H_2O catalyst, while for Fe/Mn/Mg-EG catalyst, it decreased from 0.68 to 0.61, and Fe/Mn-EG catalyst exhibit the lowest amount of higher valence state iron ion. Compared with Fe/Mn-H_2O catalyst, it can be proposed that the ethylene glycol pretreatment catalyst exhibited the higher reducibility, as it had the smaller iron particle size, higher BET surface area, and relative weak Fe–Mn interaction. However, the Mg-promoted Fe/Mn/Mg-EG catalyst showed the smallest iron particle size, but the reduction degree of the catalyst was lower than that of un-promoted catalyst. In view of the effect of the coexisting magnesium, it was considered that present of Fe–Mg interaction adjusted properties of obtained catalyst, including the reducibility, as confirmed by XPS and TPR results.

FTS performance

Activity and stability

The prepared iron-based catalysts were applied to the FTS reaction to investigate the promotional effects of ethylene glycol pretreatment on the catalytic activity and selectivity, and the variations in CO conversion with the time on stream are shown in Fig. S7. For all of the catalysts, The CO conversion increased gradually at the initial stage and reached a steady state within 7 h and then the CO conversion remains constant with the time on stream. Riedel et al. [38] studied that time on stream had dominant influence on composition and structure of the catalyst. It took several episodes for the reduced fresh iron catalyst to construct the actual catalytic phase and reach the steady state. They concluded that the FTS activity of iron catalysts was generated with time, when the α-Fe reacted with carbon from CO dissociation and formed the iron carbide (particularly Fe_5C_2), which was addressed as the true active species for FTS. It agrees well with the results in the present work. Similar results were also obtained by Yang [10] and Zhang [39].

As shown in Fig. S7 and Table 1, the Fe/Mn-EG catalyst with the larger surface area exhibited the higher activity compared with the Fe/Mn-H_2O catalyst, although the two catalysts show no difference in stability, indicating that more active sites for the FTS reaction can be provided for the highly dispersed nano-catalyst. In general, large specific surface area favors high dispersion and obtains small particle size of the active metal component, and creates more active sites, leading to a high catalytic conversion [39]. Ding et al. [7] prepared Fe_2O_3-Al_2O_3 high dispersed nano-catalysts and obtained higher FTS activity compared with conventional iron-based catalysts, they ascribed this to more active sites for the reaction can be provided for the nano-catalysts. In addition, the pore structure of the catalyst has an important influence on the catalytic performance. Li Fan et al. [40] studied the relationship between the catalyst pore structure and the catalytic activity; their results indicated that the catalyst pore size can control the catalytic activity because of the differences in the diffusion of both reactants and products. In the current study, as indicated by the N_2 physisorption results, the precursors pretreated by ethylene glycol decrease the size

of metal oxide nanoparticles and increase the average pore size. In general, the small pore size results in poor intra-pellet diffusion efficiency of reactants and products while the large pores lead to a high diffusion rate of reactants and products. Thus, it is reasonable for the high activity of the Fe/Mn-EG catalyst. This result is also in good agreement with the DRIFT characterization, which indicated the total CO adsorption for Fe/Mn-EG catalyst is higher than that for Fe/Mn-H_2O catalyst.

It is also found that the catalysts modified by magnesium exhibited lower catalytic activity than the Fe/Mn-EG catalyst in FTS reaction. The decrease in activity partly relates to a decrease in catalyst surface area as confirmed by the N_2 physisorption results. A decrease in activity could also be a result of the magnesium enriching in the surface and covering Fe active sites, hence lowering the Fe reduced, as concluded above. It may also be that a suppression of the reduction and carburization properties of the catalyst (H_2-TPR and CO-TPR results) due to the presence of the Fe–Mg interaction is responsible for a decrease in the catalyst's activity.

Product selectivity

The hydrocarbon distributions of all catalysts are listed in Table 2 and Fig. S8, the hydrocarbon selectivity were calculated using reaction data at 15 h. For catalysts prepared using ethylene glycol, the hydrocarbon product distribution shifts to the lower molecular weight hydrocarbons (C_2–C_4). It has been already pointed out that the propagation of the carbon–carbon chain occurred more easily on the catalyst with lower specific surface area where metallic particle size was larger [41], while smaller metallic particle size led to lower chain growth probability. The chain growth probability of the two catalysts was 0.90 and 0.70, respectively. The chain growth probability can be affected by many factors, such as pore resistance time and metal particle size. Here, small metal particles lower chain growth probability, and fast diffusion rates of hydrocarbons inside larger pores also decrease it. It is considered that the combination of many factors leads a remarkably decrease in the chain growth probability for Fe/Mn-EG catalyst. Based on the information given

Table 2 FTS reaction performances of iron-based catalysts in the fixed-bed reactor

Catalyst	CO conversion (%)	CO_2 selectivity[a] (%)	Hydrocarbon selectivity (c-mol%)[b]				*Ole/para*	α^c
			CH_4	$C_2^=$–$C_4^=$	C_2–C_4	C_{5+}	C_2–C_4	
Fe/Mn-H_2O	65.8	24.6	10.5	21.4	37.9	51.6	1.30	0.90
Fe/Mn-EG	83.5	34.1	7.4	34.3	47.8	44.7	2.54	0.70
Fe/Mn/Mg-EG	70.0	26.2	16.4	50.1	65.2	18.3	3.32	0.68

Reaction conditions: 553 K, 1.0 MPa, W/F = 5 g h/mol, weight of catalyst = 0.5 g

[a] Calculated from TCD, hydrocarbon free

[b] Calculated from FID

[c] Chain growth probability

above, it is indicated that the chain propagation reaction is restrained on the highly dispersed Fe/Mn-EG catalyst.

Furthermore, for Fe/Mn-EG catalyst, the ethylene glycol pretreatment increased twofold the ratio of olefin to paraffin ($C_2^=$–$C_4^=$/C_2^0–C_4^0) in the products, compared with non-pretreated iron-based catalyst. The lower olefin selectivity is increased from 21.4 to 34.3 %, and the selectivity of CH_4 decreased from 10.5 to 7.4 %. It was previously reported [40] that 1-olefins are generally produced as primary products in FTS, and are successively hydrogenated to paraffin. However, they can reabsorb onto metallic sites to receive secondary hydrocracking, breaking the terminal double-bond and releasing methane in the FTS reaction. When the pore size was larger, the transportation of the primary product was more effective and relevantly methane formation rate from secondary hydrocracking of olefins was lower. In addition, the Mn promoter enriched in the surface for Fe/Mn-EG catalyst also promoted the olefin selectivity, and this result was supported by other researchers [2, 11, 25].

As compared in Table 2, the selectivity to heavy hydrocarbons (C_5+) was successfully suppressed, whereas that to light hydrocarbons (C_2–C_4) was enhanced by the incorporation of magnesium. The addition of magnesium suppresses the chain growth ability of catalysts, and the α value decreased from 0.70 to 0.68. In addition, the selectivity of light olefins ($C_2^=$–$C_4^=$) on the Fe/Mn/Mg-EG catalyst significantly increased from 34.3 to 50.1 %, and the ratio of olefin/paraffin ($C_2^=$–$C_4^=$/C_2^0–C_4^0) also increased. The results indicated that magnesium is an effective promoter to shift product selectivity to lighter molecular weight hydrocarbons and olefins, especially for C_2–C_4 products. Yang et al. [10] found that MgO is an effective promoter in shifting FTS selectivity to lighter molecular weight hydrocarbons. Gallegos et al. [13] also found that addition of Mg increases the selectivity to all olefins on the Fe/SiO_2–MgO catalysts for FTS reaction. In addition, the Fe/Mn/Mg-EG catalyst presents no bridge CO adsorption, but stronger linear CO adsorption. It is considered that a high concentration of linear CO species would possibly lead to a high selectivity of olefin, especially light olefin, because these species rigorously suppress the hydrogenation reaction on the catalyst surface. On the other hand, for this catalyst, the adjusted reducibility both of Cu and Fe oxide, and relatively higher electron density of Fe, could contribute to suppress hydrogenation of formed light olefins resulting in the highest selectivity of light olefins.

Conclusion

The effects of ethylene glycol pretreatment on the precipitated iron-based FTS catalysts were systemically studied in this work. Iron-based catalyst pretreated by ethylene glycol leads to a smaller precipitate size and higher BET surface areas. The pretreatment of ethylene glycol can promote the reduction and accelerate the carburization of the catalyst. During the FTS reaction, the Fe/Mn-EG catalyst has higher activity and enhanced selectivity to light hydrocarbons, the chain growth ability was significantly suppressed. Furthermore, the Fe/Mn-EG catalyst realized

twofold the ratio of olefin to paraffin ($C_2^=$–$C_4^=$/C_2^0–C_4^0) than conventional iron-based catalyst.

The Mg was added to Fe/Mn-EG catalyst as a promoter. The Fe–Mg interaction reduced the crystal size and restrained the reduction and carburization, leading to decreased hydrogenation activity compared to Fe/Mn-EG, contributing to forming more light olefins. The catalyst Fe/Mn/Mg-EG realized a high CO conversion of 70 %, the highest light olefin selectivity of 50.1 % with the highest olefin/paraffin ratio of 3.32.

Acknowledgments Financial support from the National Natural Science Foundation of China (Nos. 91334206 and 51174259), Ministry of Education (NCET-13-0653), National "863" program of China (Nos. 2012AA051001 and 2013AA031702) is greatly appreciated.

Conflict of interest The authors declare no competing financial interest.

References

1. Dry ME (2002) Catal Today 71:227
2. Zhang QH, Kang JC, Wang Y (2010) ChemCatChem 2:1030
3. Galvis HMT, Bitter JH, Khare CB, Ruitenbeek M, Dugulan AI, de Jong KP (2012) Science 335:835
4. Jin Y, Datye AK (2000) J Catal 196:8
5. Jothimurugesan K, Goodwin JG Jr, Santosh SK, Spivey JJ (2000) Catal Today 58:335
6. de Smit E, Weckhuysen BM (2008) Chem Soc Rev 37:2758
7. Dong HH, Xie MJ, Xu J, Li MF, Peng LM, Guo XF, Ding WP (2011) Chem Commun 47:4019
8. Mahajan D, Gütlich P, Stumm U (2003) Catal Commun 4:101
9. Li S, Li A, Krishnamoorthy S, Iglesia E (2001) Catal Lett 77:197
10. Yang J, Sun Y, Tang Y, Liu Y, Wang H, Tian L, Wang H, Zhang Z, Xiang H, Li YW (2006) J Mol Catal A 245:26
11. Li TZ, Yang Y, Zhang CH, An X, Wan HJ, Tao ZC, Xiang HW, Li YW, Yi F, Xu BF (2007) Fuel 86:921
12. Luo M, Davis BH (2003) Appl Catal A 246:171
13. Gallegos NG, Alvarez AM, Cagnoli MV, Bengoa JF, Marchetti SG, Mercader RC, Yeramian AA (1996) J Catal 161:132
14. Nakhaeipour A, Shahri SMK, Bozorgzadeh HR, Zamani Y, Tavasoli A, Marvast MA (2008) Appl Catal A 348:201
15. Maiti GC, Malessa R, Baerns M (1983) Appl Catal 5:151
16. Jaggi NK, Schwartz LH, Butti JB, Papp H, Baerns M (1985) Appl Catal 13:347
17. Xu JD, Zhu KT, Weng XF, Weng WZ, Huang CJ, Wan HL (2013) Catal Today 215:86
18. Herranz T, Rojas S, Perez-Alonso FJ, Ojeda M, Terreros P, Fierro JLG (2006) J Catal 243:199
19. Lv X, Chen JF, Tan Y, Zhang Y (2012) Catal Commun 20:6
20. Chen JF, Zhang YR, Tan L, Zhang Y (2011) Ind Eng Chem Res 50:4212
21. Miyakoshi A, Ueno A, Ichikawa M (2001) Appl Catal A 219:249
22. Suo H, Wang S, Zhang C, Xu J, Wu B, Yang Y, Xiang HW, Li YWJ (2012) Catalyst 286:111
23. Kaden WE, Wu T, Kunkel WA, Anderson SL (2009) Science 326:826
24. Zhang CH, Yang Y, Teng BT, Li TZ, Zheng HY, Xiang HW, Li YW (2006) J Catal 237:405
25. Tao Z, Yang Y, Zhang C, Li T, Ding M, Xiang H, Li YWJ (2007) Nat Gas Chem 16:278
26. Chen W, Fan ZL, Pan XL, Bao XH (2008) J Am Chem Soc 130:9414
27. Yang Y, Xiang H, Tian L, Wang H, Zhang C, Tao Z, Xu Y, Zhong B, Li YW (2005) Appl Catal A 284:105
28. Hexana WM, Coville NJ (2010) Appl Catal A 377:150
29. Kazansky VB, Zaitsev AV, Borovkov VY, Lapidus AL (1988) Appl Catal 40:17
30. Wielers AFH, Kock AJHM, Hop CECA, Geus JW, Van Derkraan AM (1989) J Catal 117:1
31. Sun X, Zhang X, Zhang Y, Tsubaki N (2010) Appl Catal A 377:134

32. Johnston C, Jorgensen N, Rochester CHJ (1988) Chem Soc Faraday Trans 1(84):309
33. Boellaard E, van der Kraan AM, Geus JW (1996) Appl Catal A 147:207
34. Benziger JB, Larson LR (1982) J Catal 77:550
35. Bian G, Oonuki A, Koizumi N, Nomoto H, Yamada M (2002) J Mol Catal A 186:203
36. Iglesia E, Soled SL, Fiato RA, Via GH (1993) J Catal 143:345
37. Jiang M, Koizumi N, Yamada M (2000) J Phys Chem 104:7636
38. Riedel T, Schulz H, Schaub G, Jun KW, Hwang JS, Lee KW (2003) Top Catal 26:41
39. Zhang Y, Bao J, Nagamori S, Tsubaki N (2009) Appl Catal A 352:277
40. Fan L, Yokota K, Fujimoto K (1992) AIChE J 38:1639
41. Xu B, Fan Y, Zhang Y, Tsubaki N (2005) AIChE J 51:2068